Chapter 5

Memory switching in AlAs/GaAs tunneling diodes

Memory switching refers to one of two kinds of switching phenomena observed in two-terminal devices: threshold and memory switching. Threshold switching refers to a transition to a more conductive state that is maintained so long as the voltage is greater than a minimum holding voltage. When the applied bias is removed, the device returns to its original blocking or low conductance state. Perhaps the most well known threshold switching device is the thyristor (Streetman, 1990). Memory switching on the other hand, refers to a reversible change in conductance that can be maintained even without an applied bias. The first observation of reversible, electronic memory switching is due to Simmons and Verderber (1967). They observed that thin insulating films of silicon monoxide between 200 and 3000Å thick, in which gold ions were introduced, exhibited memory switching between multiple conduction curves. The mechanism invoked to explain the observation was electron trapping in the broad band of localized states in the forbidden gap of the amorphous insulator. The trapped or stored charge alters the conduction band profile near the metal-insulator interface, thus altering the conductance. Temperature and voltage induced memory switching has also been observed in thick barrier AlAs/GaAs devices grown at low temperature (Campbell et al., 1988). In these devices, that contained 50Å thick AlAs barriers and a 50Å GaAs well, with 50Å spacer layers, the memory switching was attributed to the high density of traps in

structures grown at low temperature ($\sim 500°C$). The transition from the high impedance to the low impedance state was voltage induced, with the transition back being temperature induced. Devices grown at higher temperature ($600 - 700°C$) have not shown memory switching.

Recently, AlAs/GaAs resonant tunneling diodes that contain $N^- - N^+ - N^-$ cathode-side spacers were investigated with the intention of increasing the voltage range over which negative differential resistance is observed. The idea was that the notch formed in the N^+ region would permit significant transmission even when the resonant level fell below the virtual cathode (see discussion in Chapter 2). This would yield a smooth peak and a larger voltage over which the device exhibits negative differential resistance. Such devices, however, exhibit completely unexpected behavior. The Schrödinger-Poisson model suggests that they can exhibit multiple conduction curves that exist down to zero bias (Gullapalli et al., 1992; Gullapalli, Tsao, & Neikirk, 1993a). Experimentally, devices that contain $N^- - N^+ - N^-$ spacers exhibit memory switching (Gullapalli et al., 1992; Gullapalli, Tsao, & Neikirk, 1993b).

While the Schrödinger model suggests the existence of multiple conduction curves in devices that contain $N^- - N^+ - N^-$ spacers, it provides no information as to whether the device can switch from one state to another. To understand the memory switching, a time-dependent study is necessary. The Wigner-Poisson transport model discussed in the Chapters 3 and 4, has the necessary features to enable such a study. After discussing the experimental observation of memory switching in resonant-tunneling diodes, the phenomenon is discussed within the scope of the Wigner transport model (Gullapalli et al., 1994).

5.1 Observation of memory switching in double barrier diodes

Memory switching has been observed in two-terminal devices with a double barrier tunneling structure embedded with $N^- - N^+ - N^-$ spacers. The devices were grown in a Varian Gen II molecular beam epitaxy (MBE) system. Fabrication of mesa-isolated devices is briefly outlined here. Before metallization, the material was etched in a $2:1$ $HCl:H_2O$ solution in order to remove surface oxides and to improve ohmic contact adhesion. An array of square front-side contacts (nominal sizes ranging from 10μm $\times$ 10μm to 50μm $\times$ 50μm) were defined by liftoff, using $\sim$ 15Å$Ni/$ $\sim$ 800Å$AuGe/$ $\sim$ 150Å$Ni/$ $\sim$ 1000ÅAu metallization. The front-side contacts served as a mask during mesa isolation by an $8:1:1$ $H_2SO_4:H_2O_2:H_2O$ etch. Finally, the device structures were annealed in forming gas at 450°C for 30sec. The specific contact resistance for this process was independently measured and is between $1 \times 10^{-6}\Omega - \text{cm}^2$ and $5 \times 10^{-6}\Omega - \text{cm}^2$. Indium on the backside of the sample served as the other contact. Together with the memory switching devices, a baseline resonant-tunneling diode, discussed in Chapter 4, was always fabricated to serve as the control. In addition to the simple mesa-isolated devices, implant-isolated devices (Kyono, Dietrich, & Binari, 1993) were also tested. The smallest devices on these samples are 5μm in diameter. The large contact pads on these samples, and the lower currents in the smallest devices, afford much easier characterization with the available test equipment. More importantly, it helps in eliminating any ambiguities involved in the direct probing of small area devices. Direct current J-V characterization of the devices was performed with a Keithley 230 programmable voltage source and a Keithley 195A digital multimeter. The measurements were done using test software that enables multiple sweeps of the J-V curves. The memory switching phenomenon has also been observed on a Tektronix 577 curve tracer.

Two memory switching double barrier diodes are discussed here: one with symmetric and the other with asymmetric spacers. In both devices, the double barrier tunneling structure consists of an 18 monolayer (ML) unintentionally doped (10^{15}cm^{-3}) GaAs quantum well sandwiched between nominally symmetric 6ML, unintentionally doped AlAs barriers. First consider the symmetric device, in which the tunneling structure is surrounded on both sides by an 18ML n-type (10^{15}cm^{-3}) GaAs layer closes to the barrier, a 47ML N$^+$ (4×10^{18}cm^{-3}) GaAs layer, and finally a 65ML N (10^{15}cm^{-3}) GaAs layer. The contact regions are heavily doped (4×10^{18}cm^{-3}). During the growth of the device structure, the silicon set point determining the doping density is the same in the contact regions and the N^+ layer in the spacer. The measured room temperature J-V curves of the device are shown in Fig. 5.1. Shown here are the two most repeatable and stable conduction branches observed during multiple switching cycles. The fresh device exhibits the conduction curve labeled B, the "virgin" curve. When the voltage applied across the diode is 1.5 - 2.0 V in the third quadrant (i.e. the top contact is negative), the device switches from curve B to curve A. As the bias is swept back towards zero, the device exists in state A, which remains separated from state B all the way to zero bias. The device continues in state A across zero bias, and into the first quadrant. With the device in state A, when the applied voltage is increased to about 1.5 - 2.0 V in the first quadrant, the device reverts to curve B. The switching cycle can then be repeated. The device exhibits memory switching in that once the device is placed on one branch of its J-V characteristic, it remains on that branch even after removal of all bias. Memory has been observed for durations of several minutes to hours under both short circuit and open circuit conditions. No spontaneous transitions between branches were observed while holding the device at low voltages (-1 V to +1 V). Even though the device is nominally symmetric, there is an asymmetry in the switching pattern. For example, the device switches from the high to low conductance state predomi-

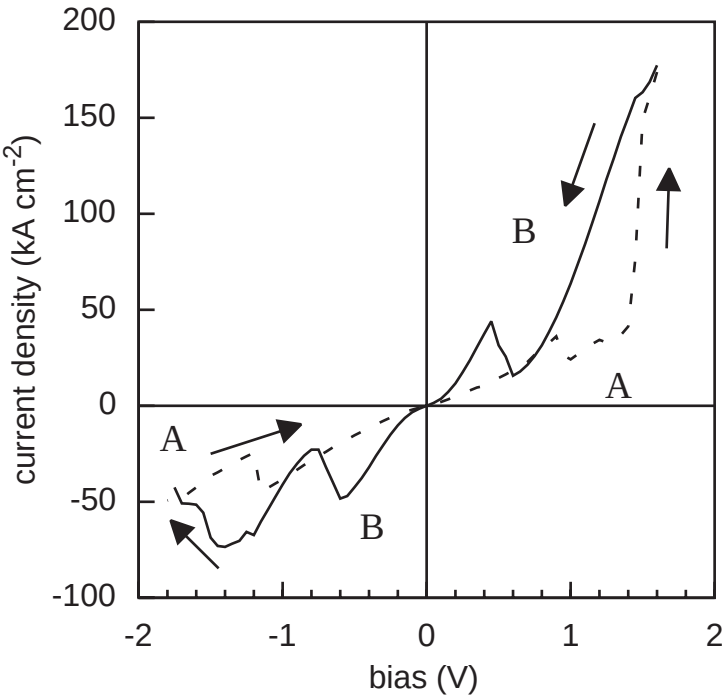

Figure 5.1: Multiple conduction curves at room temperature in a resonant tunneling diode with $N^- - N^+ - N^-$ doping profile in both the anode and cathode spacer regions. The AlAs barriers are 6ML thick and the GaAs quantum well is 18ML wide. Measurements made by the author on device structure grown by Alwin Tsao, and fabricated by Kyono, Dietrich, and Binari at the Naval Research Labs., Washington D.C.

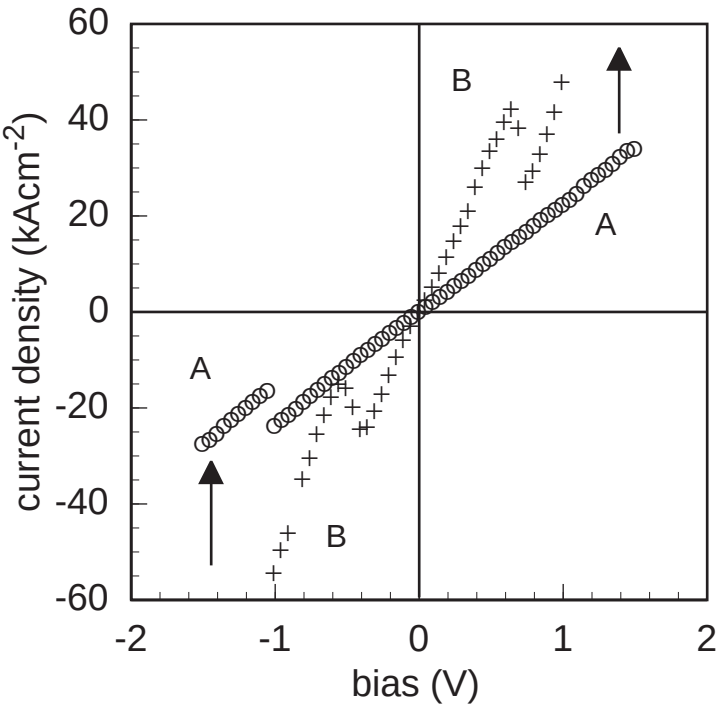

Figure 5.2: Multiple conduction curves at room temperature in a resonant tunneling diode with the $N^- - N^+ - N^-$ doping profile only in one of the spacers. The AlAs barriers are 6ML thick and the GaAs quantum well is 18ML wide. Measurements made by the author on device structure grown and fabricated by Alwin Tsao.

nantly in the third quadrant, and from the low to high conductance state in the first quadrant. A less dramatic asymmetry is in the conduction curves themselves: the peak voltages in the forward and reverse directions are different. Since the peak currents in the forward and reverse directions are similar, the asymmetry may be related to the differences in the top and bottom contacts.

In the asymmetric device, the tunneling structure is surrounded on one side by an 18ML n-type (10^{15}cm^{-3}) GaAs layer closest to the barrier, followed by a 47ML N^+ ($4 \times 10^{18}\text{cm}^{-3}$) GaAs layer, and a 65ML N (10^{15}cm^{-3}) GaAs layer. On the other side is a $26ML$ N (10^{15}cm^{-3}) GaAs layer closest to the AlAs barrier, followed by a 32ML N (10^{17}cm^{-3}) GaAs layer. The contact regions are

heavily doped ($4 \times 10^{18}\text{cm}^{-3}$). The measured room temperature J-V curves of the device are shown in Fig. 5.2. The switching behavior is similar to that exhibited by the symmetric device. The asymmetry in the J-V curves are consistent with the differences in the anode and cathode spacers, as discussed in the next section.

Conventional resonant-tunneling diodes with lightly doped spacers were also tested. The conventional diodes were grown in the same MBE system and the fabrication procedures were identical for all devices. A three-step doping transition region (as in the baseline AlAs/GaAs diode discussed in Chapter 4) comprises the spacer layers in the conventional diodes. None of the conventional quantum well diodes have shown evidence of memory switching. The current density in conventional devices is similar to the current density at which switching occurs in the memory switching devices. For this reason, thermal effects cannot be invoked to explain the observation of memory switching. Diodes with heavily doped contact regions all the way to within 50 $\mathring{A}$ of the tunneling structure were also investigated, and did not exhibit memory switching. Therefore, the switching phenomenon cannot be attributed merely to the presence of a heavily doped region in proximity to the tunneling structure. These considerations lead us to believe that essential to the phenomenon is the $\text{N}^- - \text{N}^+ - \text{N}^-$ spacer doping profile.

The negative differential characteristics of the "virgin" curve are recovered unaffected by the switching cycles. This suggests that no structural (at least not irreversible) changes occur in the active region of the device, and that the phenomenon is most probably electronic in nature. In the next section, an explanation is proposed for the memory switching phenomenon within the scope of the Wigner-Poisson model of electron transport.

5.2 Simulation of memory switching in double barrier diodes

For the purpose of simulation, we consider a double barrier tunneling structure that consists of a 18ML N^- (10^{15}cm^{-3}) GaAs quantum well sandwiched between two 6ML AlAs barriers. On one side of the tunneling structure is a lightly doped spacer consisting of 46ML N^- (10^{15}cm^{-3}) GaAs layer closest to the barrier, followed by a 32ML N (10^{17}cm^{-3}) GasAs layer. On the other side is the $\text{N}^- - \text{N}^+ - \text{N}^-$ spacer consisting of $18ML$ N^- (10^{15}cm^{-3}) GaAs layer closest to the barrier, followed by a 46ML N^+ ($2 \times 10^{18}\text{cm}^{-3}$), and 36ML N^- (10^{15}cm^{-3}) GaAs layers. The contact regions are heavily doped ($2 \times 10^{18}\text{cm}^{-3}$).

For the structure described above, the total simulation domain consists of 314 grid points in position with a mesh spacing of $a = 5.6533\text{Å}$, and 128 grid points in momentum. Since, the Wigner simulation is more difficult in the presence of the high AlAs effective-mass, for the studies on the memory switching phenomena, constant effective-mass is assumed throughout the structure. The four point, third order difference scheme, which yields excellent results when the effective-mass is constant, is used. The assumption of constant effective-mass, while affecting the magnitude of current, does not affect the main results of the study, as evidenced by calculations with the Schrödinger model.

For the device structure described above, the calculation for the Wigner distribution function results in three self-consistent charge distributions at zero bias. The solutions obtained, labeled A, B, and C, are shown in Figs. 5.3, 5.4, and 5.5. The self-consistent potentials are characterized by the different depths of the left N^+ notch, which for state A is shallow, and for state C deepest. Since the notch is close to the main quantum well, these differences also effect the position of the lowest resonance in the quantum well structure with respect to the chemical potential in the contact. Since the bottom of the quantum well is lowest in state C, the lowest resonance is closest to the contact chemical

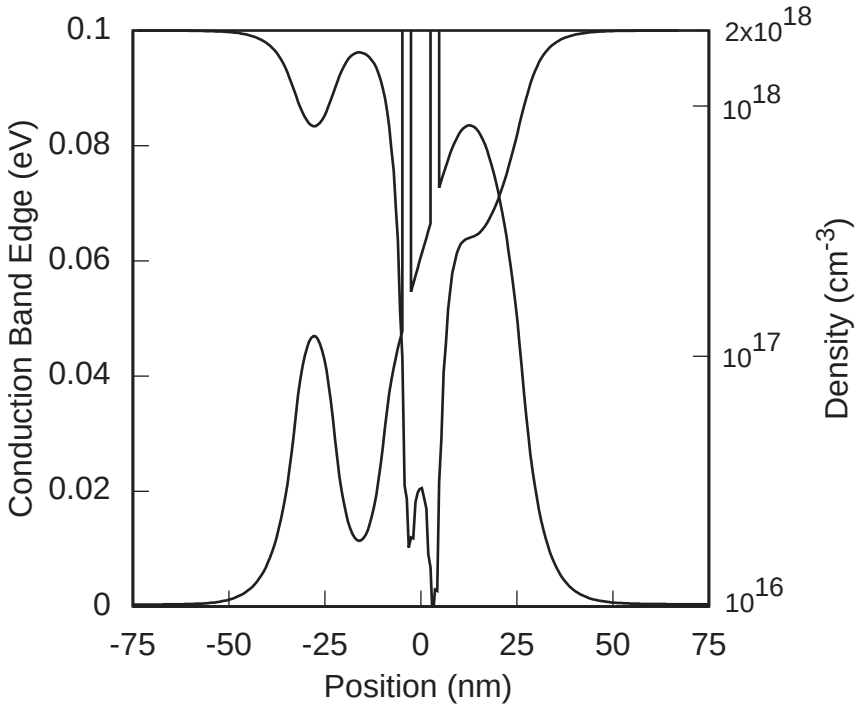

Figure 5.3: Self-consistent potential and corresponding charge distribution in state A.

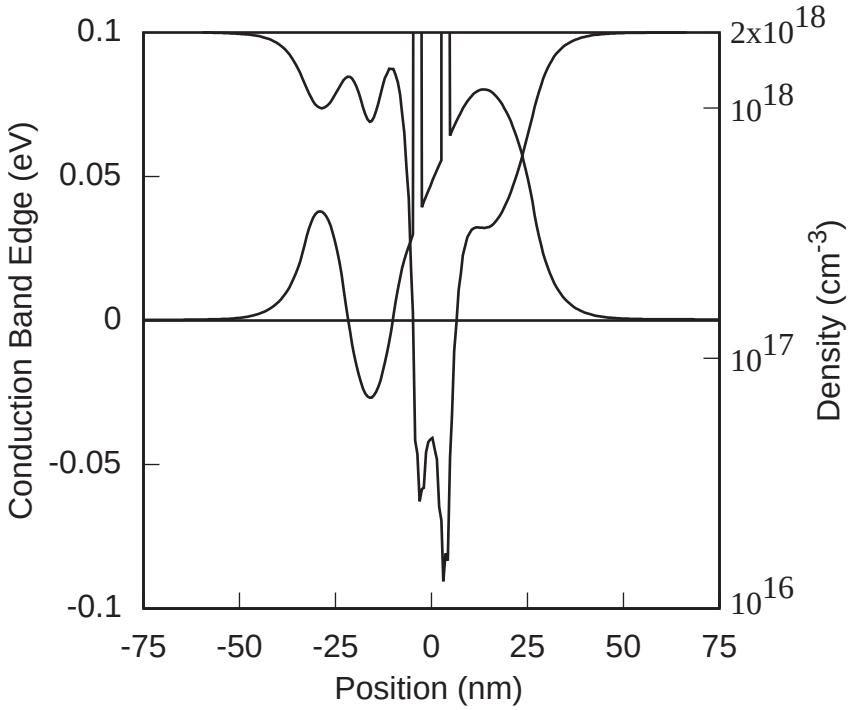

Figure 5.4: Self-consistent potential and corresponding charge distribution in state B.

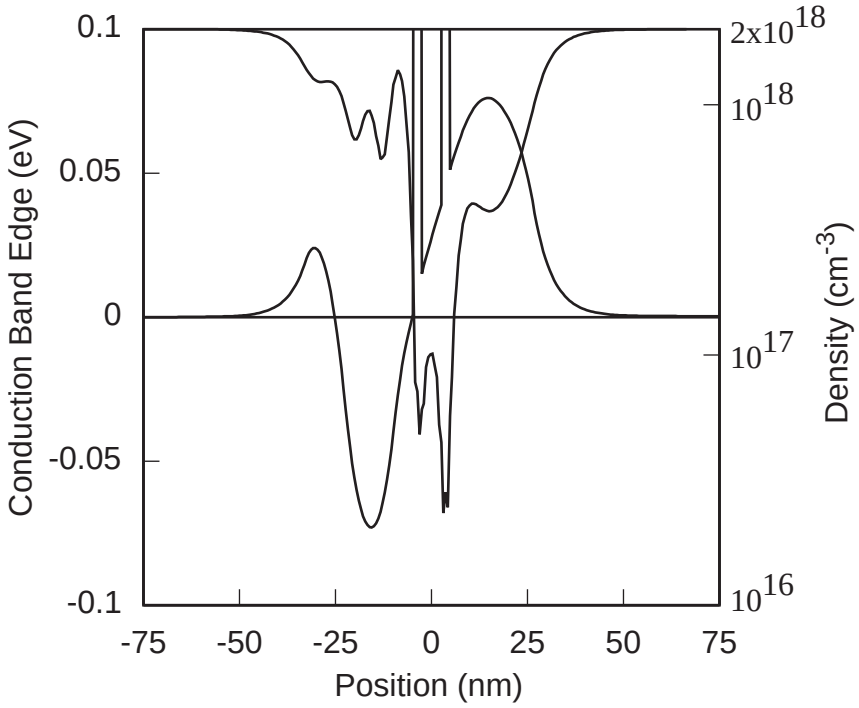

Figure 5.5: Self-consistent potential and corresponding charge distribution in state C.

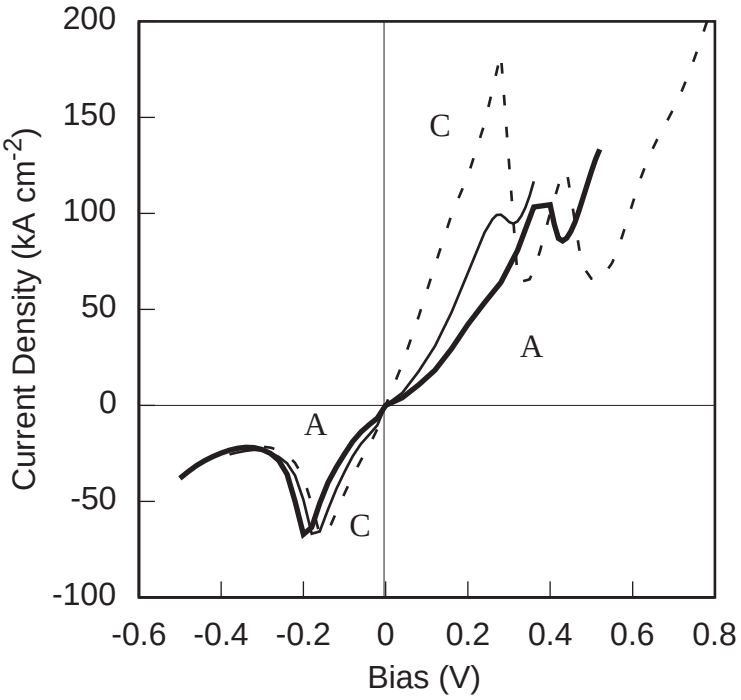

Figure 5.6: J-V curves of the memory switching resonant-tunneling diode calculated using the Wigner transport model. The left contact is taken as the reference, i.e., under forward bias the conduction band edge in the right contact is lower than that in the left. Room temperature and a distribution function relaxation time of $100fs$ is assumed. The peak currents in all three states are similar. In experiment too, the multiple conduction curves have similar peak currents.

potential, and hence more populated than in the other states. Since more electrons are available for tunneling when the resonance is closer to the contact chemical potential, the device impedance near zero bias is lowest in state C and highest in state A (assuming that the resonance widths remain similar in the two states). This is shown in Fig. 5.6.

The peak current density of the two branches are similar, at least for two of the curves, but occur at different voltages. The forward bias peak currents are almost twice the values in reverse bias. The measurements on the asymmetric device also shows these features. The peak current is higher

in forward bias than in reverse bias because the virtual cathode in the left spacer is lower than that in the right spacer, as shown in Figs. 5.3, 5.4, and 5.5. Under sufficient reverse bias, it is easy to understand that the peak currents are similar, because the charge distribution and hence the potential profile in the cathode is the same in all states. The differences in the peak voltage are accounted for by the differences in the drop across the left spacer region. That the peak currents in the forward direction are also similar is more difficult to explain.

To explore the solutions further, the zero bias Wigner distribution functions in the active region of the device for the different states are shown in Figs. 5.7, 5.8, and 5.9. Solution A is "normal" in the sense that the Wigner function looks classical. Solutions B and C, however, are unusual. The distribution functions in the three states at the left N^+ notch are shown more clearly in Fig. 5.10. The oscillations in momentum are not spurious. The proper interpretation of solutions B and C becomes clear by examining the Wigner functions corresponding to the pure states in an infinite quantum well. For the nth quantized level in an infinite quantum well of width L, the Wigner function is

$$f_n(z,k) \propto \left[\frac{\sin{(k-n\pi/L)L}}{2(k-n\pi/L)L} - (-1)^n \cos{(2\pi nz/L)}\frac{\sin kL}{kL} + \frac{\sin{(k+n\pi/L)L}}{2(k+n\pi/L)L}\right]$$

For $n = 1$, $n = 2$, and $n = 3$, the Wigner functions at the center of the infinitely deep quantum well are shown in Fig. 5.11 On comparing Figs. 5.10 and 5.11, it is clear that in state A, the Wigner function in the left N^+ notch reflects the occupation of the "ground" level, whereas in states B and C, it reflects the occupation of the first and second "excited" levels in that region. In state A, the low lying levels in the left N^+ notch are accessible while in states B and C, the lower energy states in this region are not accessible.

For the potential to be self-consistent, the charge density should respond to potential perturbations in such a way as to oppose the potential changes.

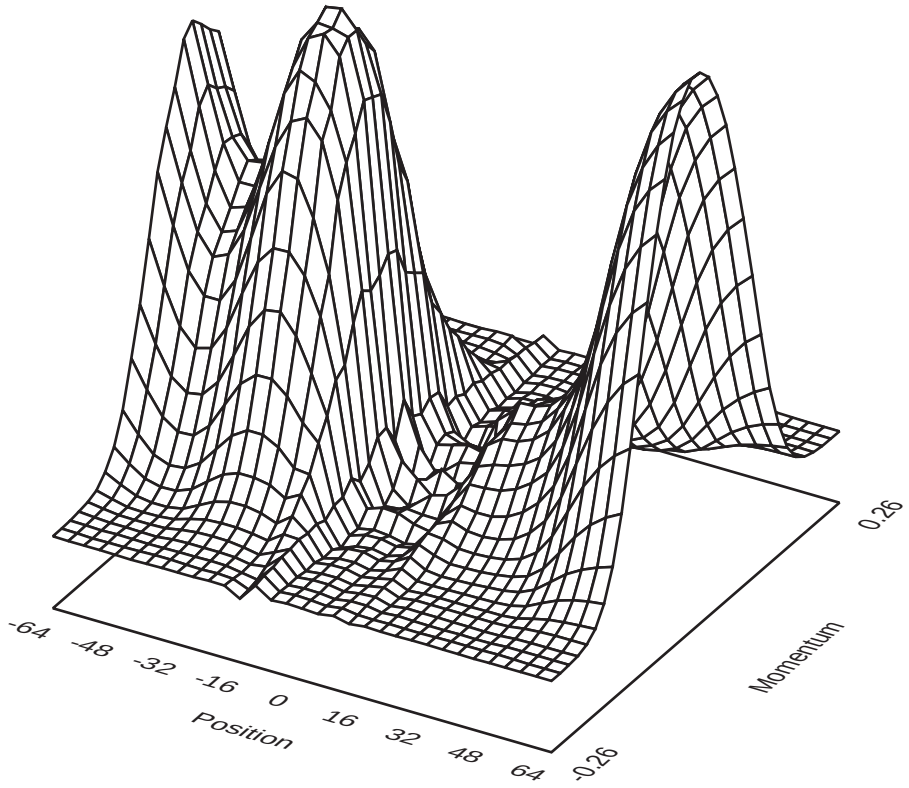

Figure 5.7: Wigner function in state A. The position is units of a and the Wigner function is shown over a quarter of the Brillouin zone.

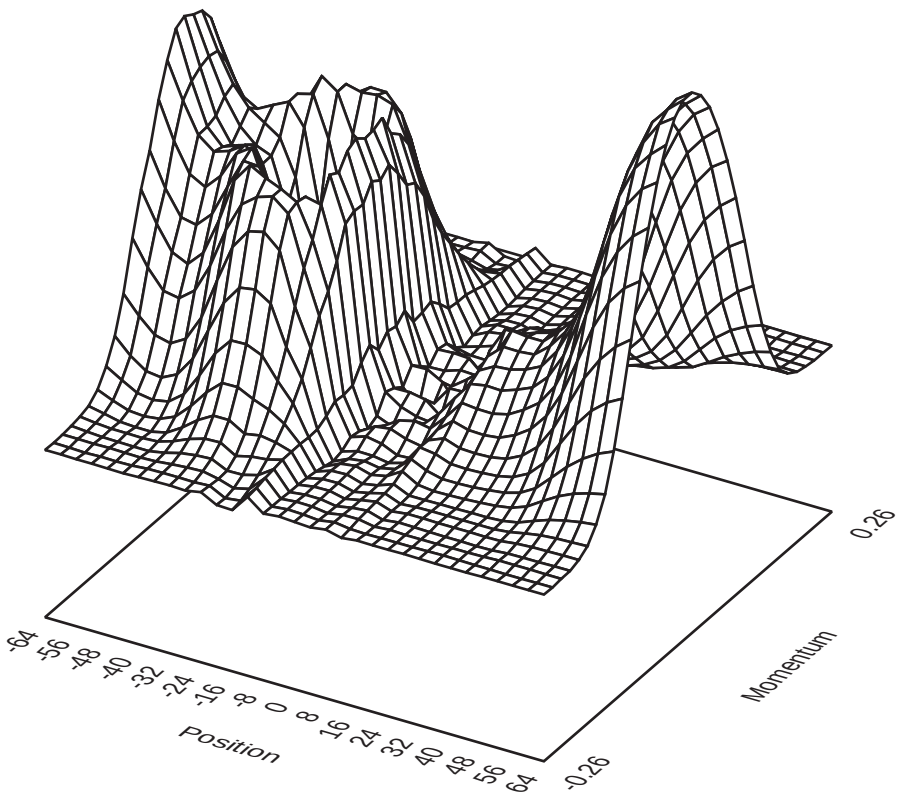

Figure 5.8: Wigner function in state B. The position is units of a and the Wigner function is shown over a quarter of the Brillouin zone.

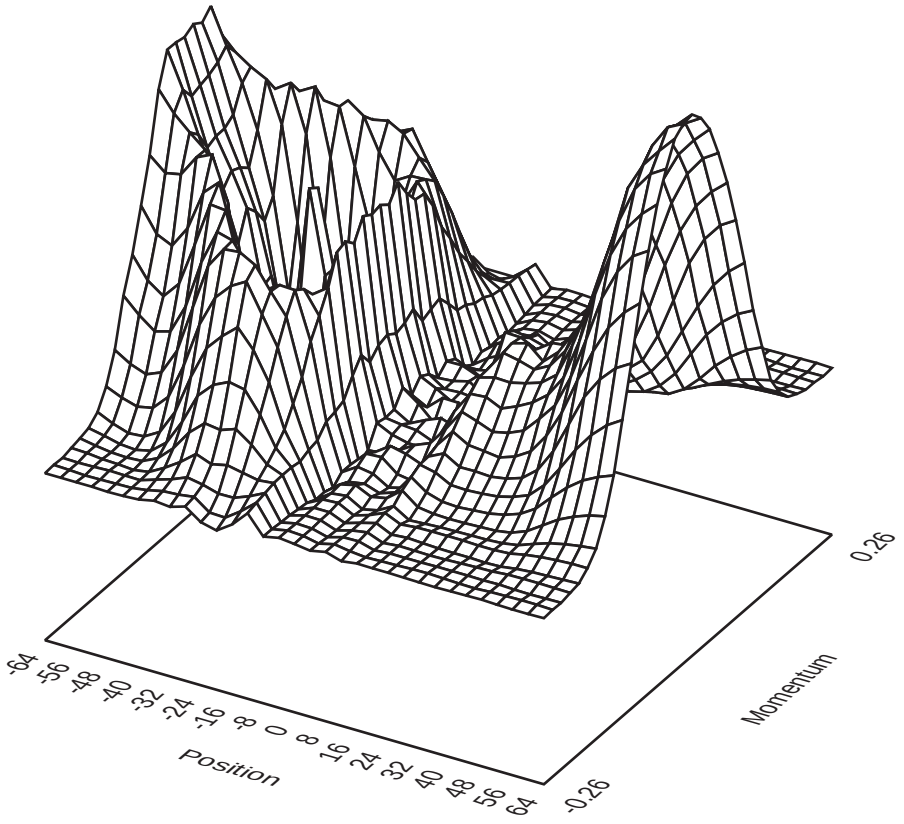

Figure 5.9: Wigner function in state C. The position is units of a and the Wigner function is shown over a quarter of the Brillouin zone.

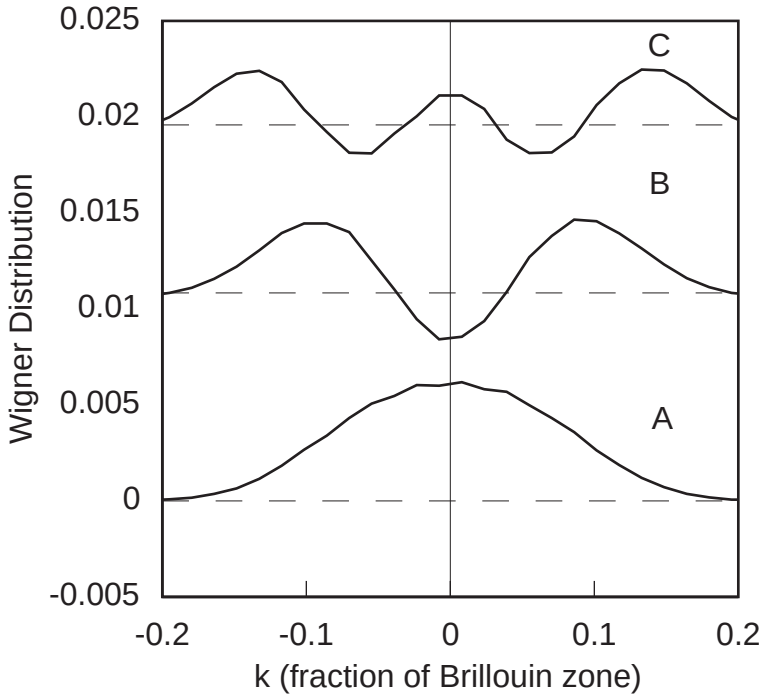

Figure 5.10: Wigner functions at the center of the left N^+ notch for the device in states A, B, and C.

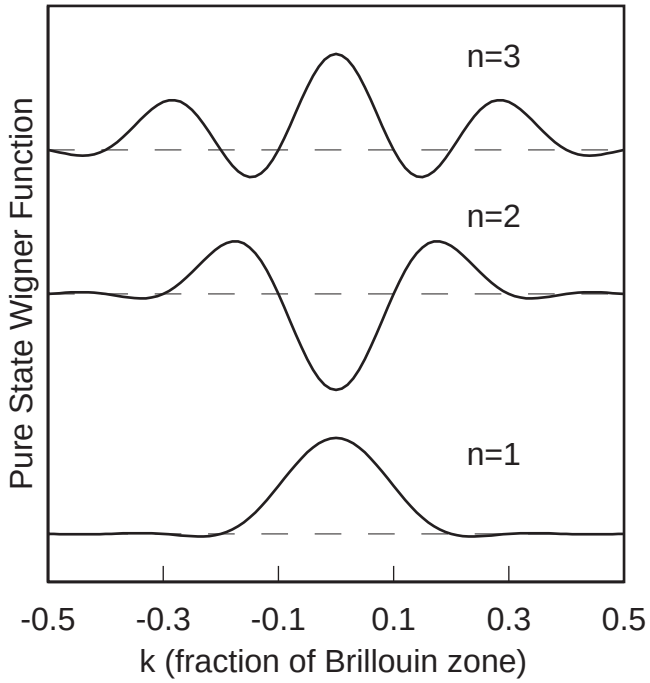

Figure 5.11: Wigner functions at the center of an infinitely deep quantum well, for the ground, first, and second excited states.

This condition is satisfied for the three solutions presented here. To switch from state A to B, for example, requires a perturbation that takes the device into the vicinity of the stable point corresponding to state B. Under the right conditions, the device can then settle in state B.

Experimentally, the individual conduction curves are stable at low bias. Transitions between the different conduction curves occur at high bias. To understand the switching phenomenon, a time-dependent simulation within the Wigner model can be used. Since the relaxation time approach is valid only near equilibrium, a proper study of the dynamics of switching requires a rigorous treatment of electron-phonon scattering away from equilibrium. If a relaxation time approach is adopted, it is easy to see that starting from one state, say A, with the corresponding equilibrium distribution f_A^{eq} entering the collision term, it is not possible to reach states B or C. This is because the collision term $(f - f_A^{eq})/\tau$ vanishes only for state A. Of course, this does not mean that other stable states cannot be reached. If the relaxation rate is weak compared to the potential, then states close to B or C will be stable for arbitrarily long periods. However, they will not correspond to thermal equilibrium states since they do not satisfy detailed balance (vanishing of collision term). Since the stability of the other states depends on the relaxation rate, this suggests that memory switching will not be observable at high temperature. But, room temperature measurements indicate otherwise. Clearly, a more general treatment of relaxation processes is required. In the absence of such a treatment, here, the time-dependent simulation is done without including the effects of collisions, and can be viewed as a low temperature study. To determine if collisions are essential to the description of the switching mechanism, low temperature measurements must be performed. Observation of memory switching at low temperatures will suggest that collisions are not essential to the switching mechanism and justify the omission of electron-phonon scattering in the following time-dependent simulation.

To show that starting in state A the device can access other states, the switching transient is self-consistently simulated with the device initially at zero bias and in state A. This is the lowest current state. The bias across the device is increased to $1.0V$ at $t = 0$, and after about $1ps$, returned to $0.0V$. An implicit time-stepping

$$\sum_{j'n'} \left[\mathcal{L}^{t+1}_{jn;j'n'} - \frac{I}{\Delta_t} \right] f^{t+1}_{j'n'} = b_{jn} - \frac{f^t_{jn}}{\Delta_t}$$

is performed, with the potential at time $t+1$ being determined self-consistently to within $10^{-3}eV$. As the simulation proceeds, the potential at $t + 1$ is self-consistent to within $10^{-4}eV$, and to the end, the potential at each time step is obtained with much greater accuracy. The time step Δ_t is chosen to be $2--5$fs. There is considerable scope for improving the efficiency of the time-dependent simulation.

Figure 5.12 shows the current transient. The charge densities in the left N^+ notch at selected points during the transient are shown in Fig. 5.13 and demonstrates that the device has switched from state A to state B. At high bias, the lower energy levels in the left N^+ notch become emptied, and as the device is returned to zero bias, the local ground level in the N^+ notch remains empty. A negative bias of $-1.0V$ can then be used to fill the N^+ notch and put the device back in state A. Figure 5.14 shows the current transient in this process. The charge densities in the left N^+ notch at selected points during the transient are shown in Fig. 5.15 and demonstrates that the

The highest current state C is difficult to access. Accessing state C in the simulation may be possible at voltages much larger than 1.0V, but this has not been investigated. While the simulations indicate the possibility of very high speed switching, the switching speed has not yet been determined experimentally.

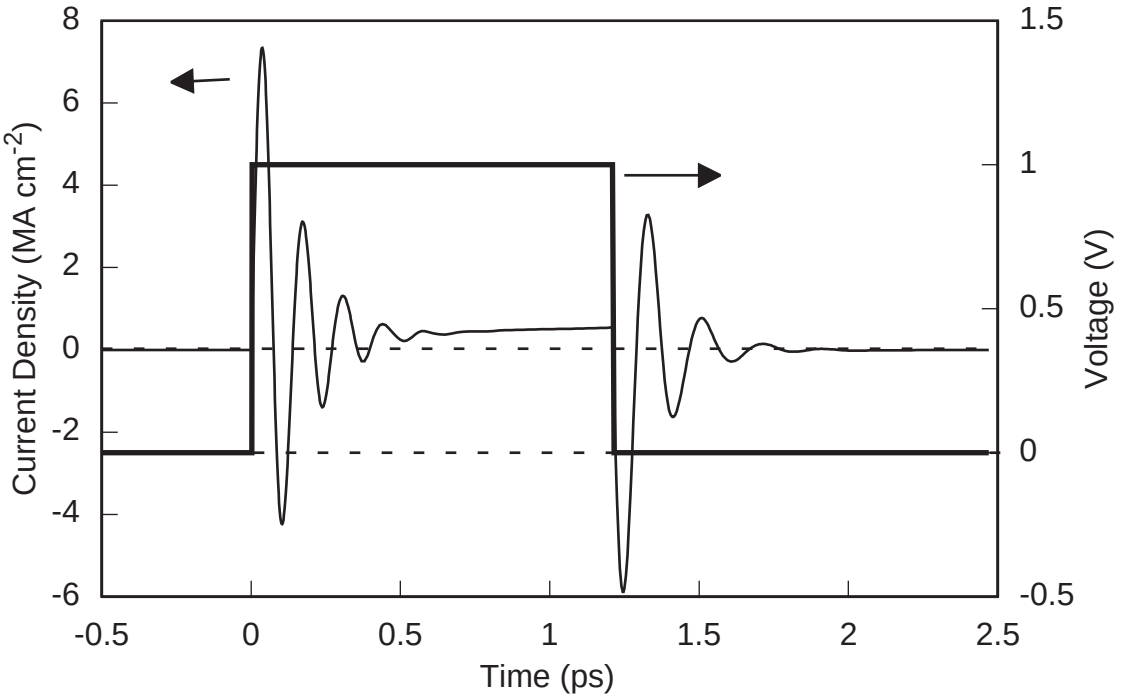

Figure 5.12: Switching transient. The device is initially in the lowest current state A. At $t = 0$, a $1V$ step is applied and in about 1ps the device is brought back to $0V$. At the end of the switching transient, the device is in state B.

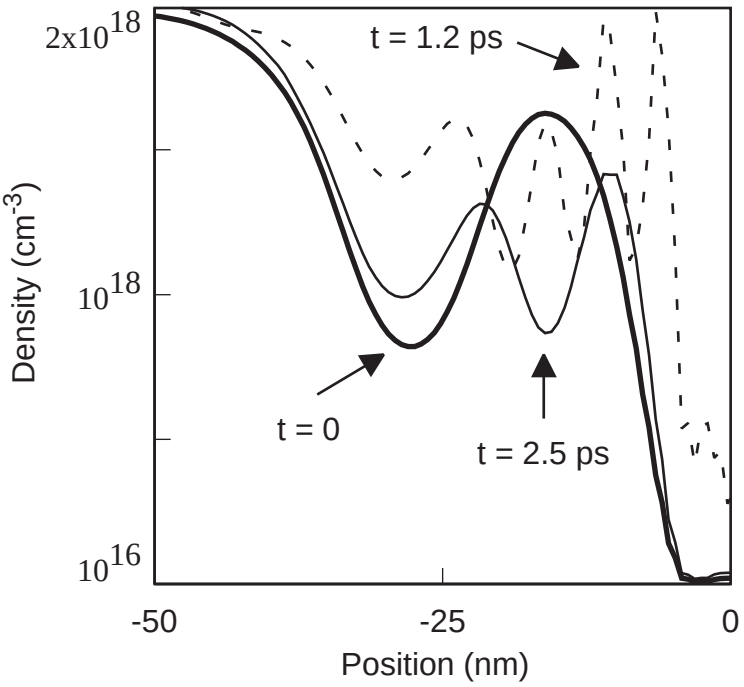

Figure 5.13: Charge density in the N^+ notch during the switching transient shown at $t = 0$, $t = 1.2$ps, and $t = 2.5$ps. At $t = 0$, the device is in state A. $t = 1.2$ps marks the end of the $1V$ pulse, and as evidenced by the oscillating charge density in the N^+ notch, the low lying energy states corresponding to the N^+ notch are emptied. At $t = 2.5$ps, near the end of the transient, the device is in state B.

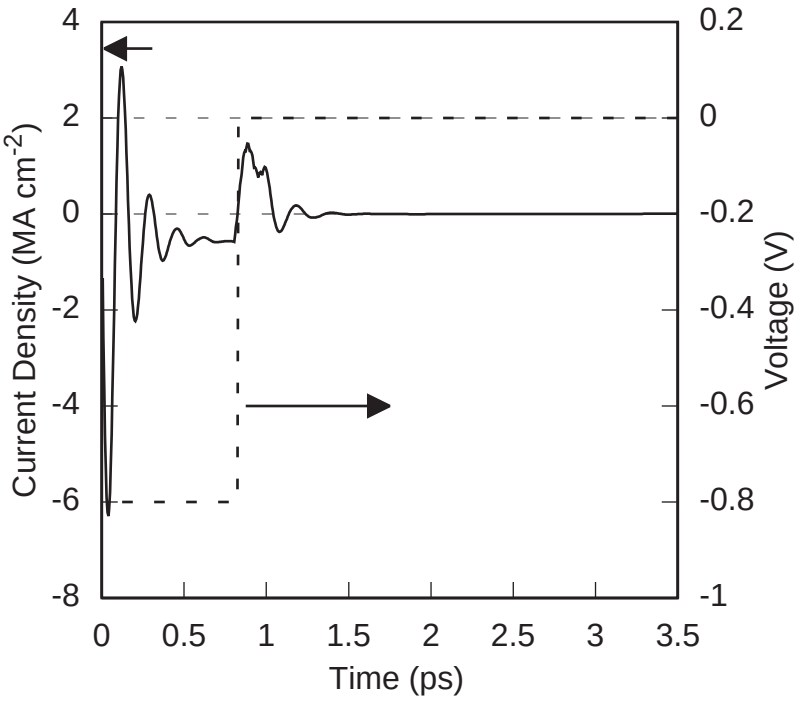

Figure 5.14: Switching transient. The device is initially in state B. At $t = 0$, a $-0.8V$ step is applied and in about 1ps the device is brought back to $0V$. At the end of the switching transient, the device is in state A. The evolution of the charge distribution during the switching transient is shown in another figure.

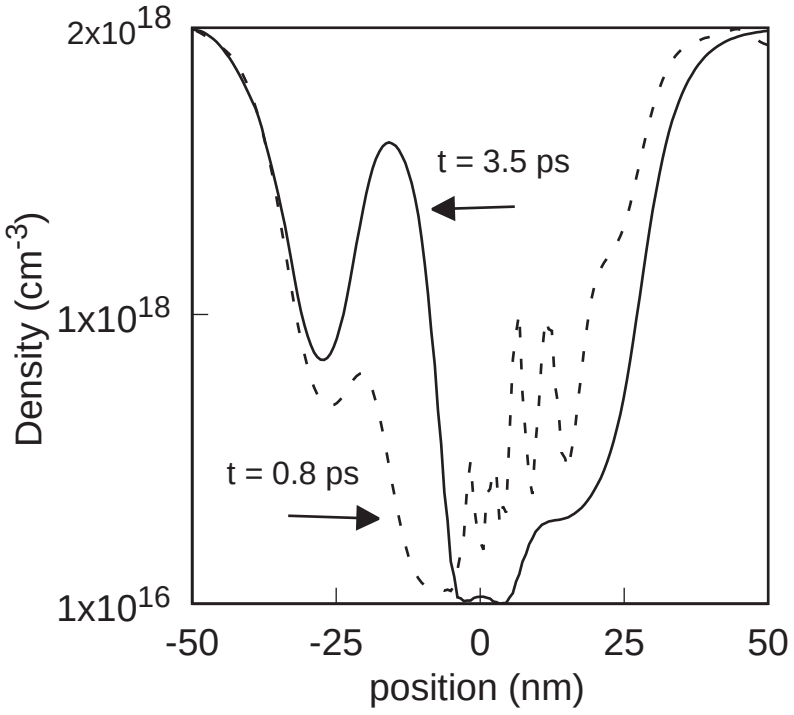

Figure 5.15: Charge density in the N^+ notch during the switching transient shown at $t = 0.8$ps and $t = 3.5$ps. The device is in state B at $t = 0$. This is the state at the end of the forward bias transient. $t = 0.8$ps marks the end of the -0.8V pulse. At $t = 3.5$ps, near the end of the transient, the device is in state A.

5.3 Summary

Memory switching phenomenon in double barrier diodes that incorporate $N^- - N^+ - N^-$ spacer layers can be understood in terms of the multiple self-consistent charge distribution predicted by the Wigner transport model. The quantum transport models used here yield multiple solution only in devices that incorporate $N^- - N^+ - N^-$ doping profile in the vicinity of a tunneling structure; experimentally too, we have observed memory switching only in such devices. The ratio of the zero bias impedance in the different states depends on the shift in the quantum well resonant level (and the associated differences in the resonance widths) due to the differences in the N^+ notch depth in the corresponding states. That the device can relax towards equilibrium on two different branches depending on its preparation far from equilibrium is intriguing. A time-dependent simulation of the Wigner transport equation, ignoring collisions, suggests that at high bias the device can switch from one conduction curve to the other, and when allowed to relax to equilibrium (or zero bias), it does so on a different conduction curve. A key to further understanding of this device will be a rigorous treatment of dissipative processes such as electron-phonon scattering in quantum devices, a subject of much current research interest. To clarify the importance of collisions in memory switching, low and high temperature experiments would be useful. In the absence of collisions, the temperature dependence of the conduction curves is only due to the boundary condition on the distribution. The switching speed and device behavior in response to periodic train of switching pulses also needs to be studied. In conjunction with small signal analysis based on the time-dependent Wigner equation, the measurement of the impedance of the device at zero bias can yield insight into the charge distributions in the different devices. Work in this direction will depend on the design of low current density memory switching devices.